European Conference on Optical Communication (ECOC) 2022 © Optica Publishing Group 2022

Slice-Less Optical Arbitrary Waveform Measurement (OAWM) on a Silicon Photonic Chip

Daniel Drayss[1,2], Dengyang Fang[1], Christoph Füllner[1], Artem Kuzmin[3], Wolfgang Freude[1], Sebastian Randel[1] and Christian Koos[1,2]

[1] Institute of Photonics and Quantum Electronics, Karlsruhe Institute of Technology (KIT), Germany,
[2] Institute of Microstructure Technology, Karlsruhe Institute of Technology (KIT), Germany,
[3] Laboratory for Applications of Synchrotron Radiation, Karlsruhe Institute of Technology (KIT); Germany
daniel.drayss@kit.edu, christian.koos@kit.edu

Abstract *We demonstrate the first slice-less optical-arbitrary-waveform-measurement (OAWM) front-end integrated on a silicon photonic chip and demonstrate its viability by reception of high-speed data signals (100 GBd 64 QAM). Our system covers a bandwidth of more than 160 GHz and exploits an accurate calibration for high-fidelity signal reconstruction. ©2022 The Author(s)*

Introduction

Optical arbitrary waveform measurement (OAWM) based on optical frequency combs gives access to the full-field information of broadband optical waveforms [1-4]. Applications range from reception of high-speed communication signals [2-4] and elastic optical networking [5] to ultra-broadband photonic-electronic analog-to-digital conversion (ADC) [6-8] and investigation of ultra-short events in science and technology [1]. Previous demonstrations of OAWM have relied on spectrally sliced reception, where the broadband optical input signal is first decomposed into a multitude of narrowband spectral slices, which are individually received by an array of in-phase/quadrature receivers (IQR) using a frequency comb as multi-wavelength local oscillator (LO). The original waveform is then reconstructed by digital stitching of the individual tributaries [1-4]. However, this scheme requires high-quality optical filters for spectral slicing of the optical signal and for separating the comb tones. While the IQR can be efficiently integrated using readily available platforms such as silicon photonics (SiP) or indium phosphide (InP), the associated high-quality slicing filters are much more challenging to implement based on high index-contrast waveguides. As an example, previous demonstrations of integrated OAWM receivers either relied on InP-based arrayed waveguide gratings (AWG), that required individual phase correction in the various arms [9], or on SiP coupled-resonator optical waveguide (CROW) structures [4,10], that need sophisticated control schemes for thermal tuning. To overcome these challenges, we recently proposed and demonstrated a slice-less OAWM scheme [11], which does not require any high-quality slicing filters. However, this experiment still relied on discrete fiber-optic components.

In this paper, we demonstrate the first integrated slice-less OAWM front-end. The scheme relies on an array of IQR, which are fed by the full optical waveform and by time-delayed copies of the full LO comb. The electrical signals then contain superimposed mixing products of the various LO tones with the respective adjacent portions of the signal spectrum and allow to reconstruct the full-field information of the incoming waveform using advanced DSP [11]. Our demonstration relies on a single silicon photonic integrated circuit (PIC) that combines an array of IQR with the associated passive components such as power splitters and delay lines. The PIC does not require any active control and is wavelength-agnostic, easily covering the telecommunication C-band. In our proof-of-concept experiments, we use four IQR and demonstrate an acquisition bandwidth of more than 160 GHz. The viability of the scheme is shown by reception of various waveforms such as a 100 GBd 64 QAM signal or a combination of 60 GBd and 80 GBd 64QAM signals. The bandwidth of the system scales linearly with the number of receiver channels and can thus be further increased. To the best of our knowledge, our experiments represent the first OAWM demonstration with an optical front-end having co-integrated photodetectors.

Concept, experimental setup, and PIC design

The concept of slice-less OAWM is illustrated in Fig. 1(a). A transmitter (Tx) generates an optical signal $\underline{a}_S(t)$, that is amplified and fed to the integrated OAWM front-end that is a silicon PIC. On the PIC, the signal is split into $N = 4$ copies and routed to an integrated IQR array (IQR 1…4). An optical frequency comb generator (FCG) generates $M = 4$ phase coherent optical tones with frequencies f_μ and with a free spectral range f_{FSR} by modulating a continuous-wave tone emitted by a low-linewidth fiber laser. The LO comb is coupled to the PIC, where it is split and delayed before being fed to the IQR array. The individual delays τ_ν are approximately evenly distributed over the repetition period of the LO. The in-phase (I) and quadrature (Q) components $I_\nu(t)$ and $Q_\nu(t)$ $(\nu = 1,\ldots N)$ of the complex-valued baseband signals are extracted from the respective balanced photodiode and digitized by an array of ADC. The

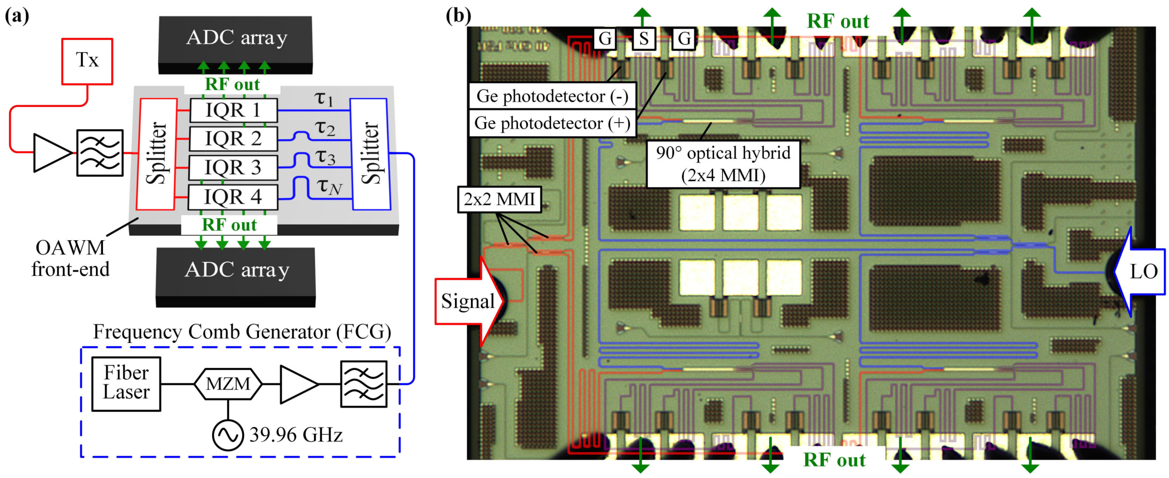

Fig. 1. Concept and implementation of an OAWM receiver front-end on a silicon photonic integrate circuit (PIC). (a) A transmitter (Tx) generates a signal that is amplified and coupled to the OAWM front-end. An optical frequency comb generator (FCG) based on a Mach-Zehnder modulator (MZM) and a low-phase-noise fiber laser generates four coherent tones spaced by $f_{\mathrm{FSR}} = 39.96\ \mathrm{GHz}$ that are used as multi-wavelength local oscillator (LO). The signal is split into four copies and routed to an array of in-phase quadrature receivers (IQR). The LO is also split, delayed by τ_ν, $\nu = 1,\ldots,4$, and also routed to the IQR array. The radio-frequency (RF) output signals are captured by an array of ADC (UXR series oscilloscopes), and the signal under test is reconstructed by digital signal processing (not shown). (b) Photograph of the OAWM PIC comprising several 2x2 multi-mode interference couplers (MMI) as power splitters, delay lines for the LO, 90° optical hybrids (2x4 MMI) as well as balanced Germanium photodetectors. The RF signals are extracted with GSG probes from the top and bottom. The BPD are biased at −3 V.

baseband signals $\underline{U}_\nu(t) = I_\nu(t) + \mathrm{j}Q_\nu(t)$ can then be related to the optical input waveform $\underline{a}_\mathrm{S}(t)$ by a frequency domain model [11]

$$\tilde{\underline{U}}_\nu(f) = \sum_{\mu=1}^{M} \tilde{\underline{H}}_{\nu\mu}(f)\,\tilde{\underline{a}}_\mathrm{S}(f + f_\mu) + \tilde{\underline{G}}_\nu(f), \quad (1)$$

where $\tilde{\underline{G}}_\nu(f)$ is statistically independent additive noise introduced by the receivers and where $\tilde{\underline{H}}_{\nu\mu}(f)$ are equivalent transfer functions that comprise both optical characteristics around the associated LO tone f_μ and electrical characteristics of the respective $\mathrm{IQR}\,\nu$. Assuming that all transfer functions are known, Eq. (1) can be inverted, and the complex-valued envelope of the optical input signal $\underline{a}_\mathrm{S}(t)$ can be reconstructed. Note that this scheme resembles so-called asynchronous time interleaving that is used in high-speed digital oscilloscopes [12],[13]. However, for the optical implementation used here, the compensation of phase drifts is critical, especially when measuring unknown arbitrary waveforms [11] rather than communication signals with known structure [14],[15]. In our experiments, these phase drifts are digitally compensated by exploiting redundant information contained in the baseband signals if the associated acquisition bandwidth exceeds $f_{\mathrm{FSR}}/2$ [11].

Fig. 1(b) shows a photograph of the OAWM PIC. The PIC comprises dedicated couplers for the signal (left) and the LO (right), which are prepared for future optical packaging with photonic wire bonds (PWB) [16]. The power splitters rely on 2x2 multi-mode interference (MMI) couplers, the 90° optical hybrids comprise 2×4 MMI that establish the desired 90° phase relationship between its paired outputs for the in-phase $I(t)$ and quadrature $Q(t)$ signals, such that no active phase shifters are required. We measure this IQ-phase for all IQR to be in the range of 84° to 89°. Each balanced photodetector (BPD) consists of two Germanium photodiodes that are reverse biased at −3 V. All channels are contacted with two 4×GSG probes and connected with 70 cm-long coaxial cables to two synchronized oscilloscopes (Keysight UXR-series) that serve as back-end ADC. The digital data is processed offline in Matlab. In all our measurements we use an LO comb with $f_{\mathrm{FSR}} = 39.96\ \mathrm{GHz}$.

Calibration

For accurate signal reconstruction, the transfer functions $\tilde{\underline{H}}_{\nu\mu}(f)$ in Eq. (1) must be determined in an independent measurement. To this end, we use a known optical reference waveform (ORW) generated by a femtosecond laser (Menhir Photonics) with a repetition rate of $f_{\mathrm{ORW}} = 250\ \mathrm{MHz}$ to spectrally sample the transfer function at discrete points spaced by f_{ORW}. The reference waveform has been characterized by a frequency-resolved optical gating (FROG) measurement. To avoid saturating the photodetectors with the high peak power of the optical pulses, we attenuate the ORW sufficiently and disperse it by adding 2×10 km of single mode fiber (SMF1 + SMF2). This reduces the peak-to-average power ratio (PAPR) of the ORW significantly and thus improves the SNR of the calibration. Note that we perform additional measurements with only SMF1 or only SMF2 in the measurement path to accurately separate the phase profile imposed by the fibers from the response of the receiver. In Fig. 3(a), we show the measured transfer function $\tilde{\underline{H}}^{(\mathrm{I})}_{1,1}(f) = \left|\tilde{\underline{H}}^{(\mathrm{I})}_{1,1}(f)\right| \exp\left(\mathrm{j}\varphi^{(\mathrm{I})}_{1,1}(f)\right)$ as an example. In contrast to the formulation in

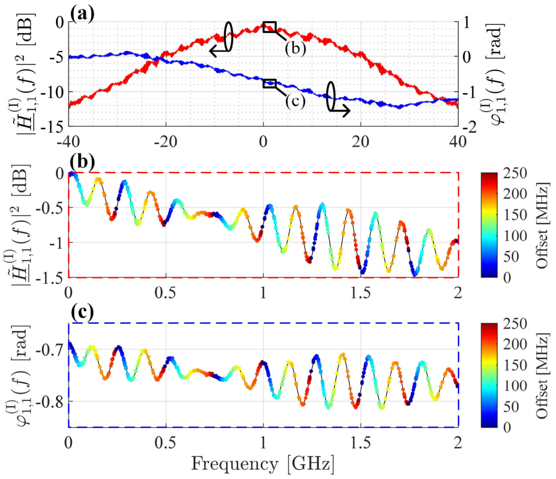

Fig. 3. Calibration of the OAWM receiver. **(a)** Power response $\left|\tilde{H}_{11}(f)\right|^2$ (red) and phase response $\varphi_{11}(f)$ (blue) of the transfer function $\tilde{H}_{1,1}^{(\mathrm{I})}(f)=\left|\tilde{H}_{1,1}^{(\mathrm{I})}(f)\right|\exp\left(\mathrm{j}\varphi_{1,1}^{(\mathrm{I})}(f)\right)$. **(b)** Zoom-in of the power transfer function from 0 to 2 GHz, see black box in (a). The individual color-coded dots represent individual calibrations, that are recorded with different frequency offsets between ORW and LO. The individual calibrations are stitched to obtain a high-resolution calibration. **(c)** Zoom-in of the phase transfer from 0 to 2 GHz, see black box in (a).

Eq.(1), we calibrate for the in-phase $\tilde{H}_{\nu\mu}^{(\mathrm{I})}(f)$ and quadrature $\tilde{H}_{\nu\mu}^{(\mathrm{Q})}(f)$ channel of each IQR separately. This allows to additionally compensate for any IQ-imbalance. The power response $\left|\tilde{H}_{11}^{(\mathrm{I})}(f)\right|^2$, red trace in Fig. 3(a), comprises the roll-off of all components (BPD, probe, cable, coaxial adaptors) and reaches −5 dB at the minimum required ADC bandwidth $B_{\mathrm{RF}} \geq f_{\mathrm{FSR}}/2 \approx 20\ \mathrm{GHz}$. The phase response $\varphi_{11}(f)$, blue trace in Fig. 3(a), is approximately flat in the bandwidth of interest. To obtain a calibration with sufficient spectral resolution, we resort to a multi-shot calibration technique, i.e., we acquire several calibrations while varying the frequency offset between the ORW and the LO. This is illustrated in a Zoom-in shown in Fig. 3(b) and (c), which depict the color-coded individual calibrations for the power and phase response after compensation of time variant phase drifts in a 2 GHz-wide spectral range, see black boxes in Fig. 2(a). Note that the fine ripples on top of the amplitude and phase response seen in Fig. 3(b) and (c) can be attributed to reflections in the 70 cm-long RF cables originating from poor matching of the high-impedance photodetectors to the 50 Ohm input of the oscilloscope. We further characterized the distortions of our OAWM system by measuring single-tone test signals. The calibration can reduce the crosstalk between different spectral bands, as well as the IQ-images to −40 dB on average. The system performance is therefore mainly limited by noise introduced in the backend ADC.

Experimental demonstration

We test the OAWM system using different optical data signals that were generated by high-speed IQ modulators and electrical arbitrary-waveform generators (M8194A from Keysight). Fig. 2(a) shows the power spectrum of a reconstructed 100 GBd 64 QAM data signal and the corresponding constellation diagram, from which we estimate the constellation SNR, $\mathrm{SNR_c} = 19.3\ \mathrm{dB}$. We believe that the performance is mainly limited by the transmitter, as we previously obtained similar results (same transmitter) for a single-slice IQ receiver and a spectrally sliced OAWM system [4]. We additionally record the electrical receiver noise with all optical signals being disconnected. After applying the same DSP to the noise recordings as previously to the actual data, we obtain the stitched receiver noise (gray) in Fig. 2(a). It has a periodic frequency dependence, as different spectral slices are stitched and as the roll-off of the IQR is digitally compensated for each slice. In Fig. 2(b) we show another example, where an 80 GBd and a 60 GBd 64 QAM signal is fit into the receiver bandwidth of slightly more than 160 GHz. Due to the lower individual bandwidths, the $\mathrm{SNR_c}$ increases to 21.3 dB and 21.9 dB, respectively. The receiver bandwidth can well compete with previous demonstrations of spectrally sliced OAWM receivers that still relied on external photodiodes [1,4].

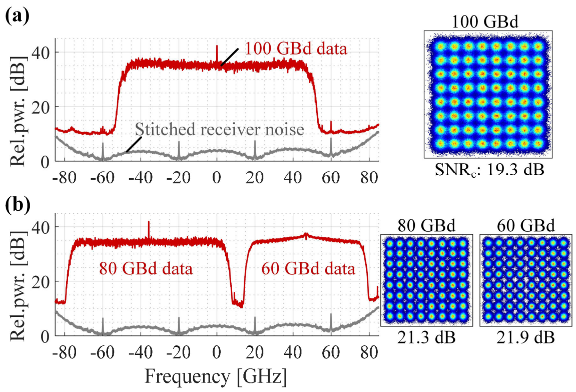

Fig. 2. Power spectrum (resolution bandwidth 100 MHz) of reconstructed data (red), stitched receiver noise floor (gray), and corresponding constellation diagrams.

Summary

We have demonstrated an OAWM front-end using an integrated silicon PIC that combines passive delay lines with the associated high-speed IQ-receivers. We achieve a total bandwidth of 160 GHz. With a high-resolution calibration, we can reduce crosstalk and IQ-images to -40 dB and obtain an accurate representation of the signal under test. The concept is further scalable to larger bandwidths.

Acknowledgements: This work was supported by the ERC Consolidator Grant TeraSHAPE (# 773248), by the EU H2020 project TeraSlice (# 863322), by the DFG projects PACE (# 403188360) and GOSPEL (# 403187440) within the Priority Programme SPP 2111, by the BMBF project Open6GHub (no. 16KISK010), by the EU H2020 Marie Skłodowska-Curie Innovative Training Network MICROCOMB (# 812818), by the Alfried Krupp von Bohlen und Halbach Foundation, by the Max-Planck School of Photonics (MPSP), and by the Karlsruhe School of Optics & Photonics (KSOP).

Disclaimer: Preliminary paper, subject to publisher revision

References

[1] N. K. Fontaine, R. P. Scott, L. Zhou, F. M. Soares, J. P. Heritage, and S. J. B. Yoo, "Real-time full-field arbitrary optical waveform measurement," Nature Photonics **4**, 248–254 (2010). DOI: 10.1038/nphoton.2010.28

[2] N. K. Fontaine, T. Sakamoto, D. J. Geisler, R. P. Scott, B. Guan, and S. J. B. Yoo, "Coherent reception of 80 GBd QPSK using integrated spectral slice optical arbitrary waveform measurement," in Conference on Lasers and Electro-Optics 2012, paper CTh1H.1, DOI: 10.1364/CLEO_SI.2012.CTh1H.1

[3] N. K. Fontaine, G. Raybon, B. Guan, A. Adamiecki, P. J. Winzer, R. Ryf, A. Konczykowska, F. Jorge, J.-Y. Dupuy, L. L. Buhl, S. Chandrashekhar, R. Delbue, P. Pupalaikis, and A. Sureka, "228-GHz Coherent Receiver using Digital Optical Bandwidth Interleaving and Reception of 214-GBd (856-Gb/s) PDM-QPSK," in European Conference and Exhibition on Optical Communication (2012), DOI: 10.1364/ECEOC.2012.Th.3.A.1

[4] Dengyang Fang, Andrea Zazzi, Juliana Müller, Daniel Drayss, Christoph Füllner, Pablo Marin-Palomo, Alireza Tabatabaei Mashayekh, Arka Dipta Das, Maxim Weizel, Sergiy Gudyriev, Wolfgang Freude, Sebastian Randel, J. Christoph Scheytt, Jeremy Witzens, and Christian Koos, "Optical Arbitrary Waveform Measurement (OAWM) Using Silicon Photonic Slicing Filters," J. Lightwave Technol., JLT **40**, 1705–1717 (2022). DOI: 10.1109/JLT.2021.3130764

[5] R. Proietti, C. Qin, B. Guan, N. K. Fontaine, S. Feng, A. Castro, R. P. Scott, and S. J. B. Yoo, "Elastic Optical Networking by Dynamic Optical Arbitrary Waveform Generation and Measurement," J. Opt. Commun. Netw. 8, A171 (2016). DOI: 10.1364/JOCN.8.00A171

[6] A. Zazzi, J. Müller, S. Gudyriev, P. Marin-Palomo, D. Fang, J. C. Scheytt, C. Koos, and J. Witzens, "Fundamental limitations of spectrally-sliced optically enabled data converters arising from MLL timing jitter," Opt. Express, OE **28**, 18790–18813 (2020). DOI: 10.1364/OE.382832

[7] A. Zazzi, J. Müller, M. Weizel, J. Koch, D. Fang, A. Moscoso-Mártir, A. T. Mashayekh, A. D. Das, D. Drayß, F. Merget, F. X. Kärtner, S. Pachnicke, C. Koos, J. C. Scheytt, and J. Witzens, "Optically enabled ADCs and application to optical communications," IEEE Open Journal of the Solid-State Circuits Society, **1** (2021). DOI: 10.1109/OJSSCS.2021.3110943

[8] D. Fang, D. Drayss, G. Lihachev, P. Marin-Palomo, H. Peng, C. Füllner, A. Kuzmin, J. Liu, R. Wang, V. Snigirev, A. Lukashchuk, M. Zhang, P. Kharel, J. Witzens, C. Scheytt, W. Freude, S. Randel, T. J. Kippenberg, and C. Koos, "320 GHz Analog-to-Digital Converter Exploiting Kerr Soliton Combs and Photonic-Electronic Spectral Stitching," in European Conference on Optical Communication (2021), DOI: 10.1109/ECOC52684.2021.9606090

[9] N. K. Fontaine, R. P. Scott, and S. Yoo, "Dynamic optical arbitrary waveform generation and detection in InP photonic integrated circuits for Tb/s optical communications," Optics Communications **284**, 3693–3705 (2011). DOI: 10.1016/j.optcom.2011.03.045

[10] J. Müller, A. Zazzi, G. Vasudevan Rajeswari, A. Moscoso Martir, A. Tabatabaei Mashayekh, A. D. Das, F. Merget, and J. Witzens, "Optimized hourglass-shaped resonators for efficient thermal tuning of CROW filters with reduced crosstalk," IEEE 17th International Conference on Group IV Photonics (GFP) (2021), DOI: 10.1109/GFP51802.2021.9673904

[11] D. Drayss, D. Fang, C. Füllner, G. Likhachev, T. Henauer, Y. Chen, H. Peng, P. Marin-Palomo, T. Zwick, W. Freude, T. J. Kippenberg, S. Randel, and C. Koos, "Slice-Less Optical Arbitrary Waveform Measurement (OAWM) in a Bandwidth of More Than 600 GHz," in Optical Fiber Communications Conference and Exhibition (2022), DOI: 10.1364/OFC.2022.M2I.1

[12] Tektronix, "Techniques for Extending Real-Time Oscilloscope Bandwidth", White Paper 55W-29371-3 (2015), http://www.tek.com/document/whitepaper/techniques-extending-real-time-oscilloscope-bandwidth

[13] Tektronix, "DPO70000SX Series Datasheet" , Datasheet (last accessed 2022) https://download.tek.com/manual/DPO70000SX-Series-Real-Time-Oscilloscopes-User-Manual-EN-071335707.pdf.

[14] X. Chen, X. Xie, I. Kim, G. Li, H. Zhang, and B. Zhou, "Coherent Detection Using Optical Time-Domain Sampling," IEEE Photonics Technology Letters **21**, 286–288 (2009), DOI: 10.1109/LPT.2008.2010868

[15] J. K. Fischer, R. Ludwig, L. Molle, C. Schmidt-Langhorst, C. C. Leonhardt, A. Matiss, and C. Schubert, "High-Speed Digital Coherent Receiver Based on Parallel Optical Sampling," Journal of Lightwave Technology **29**, 378–385 (2011), DOI: 10.1109/JLT.2010.2090132

[16] M. Blaicher, M. R. Billah, J. Kemal, T. Hoose, P. Marin-Palomo, A. Hofmann, Y. Kutuvantavida, C. Kieninger, P.-I. Dietrich, M. Lauermann, S. Wolf, U. Troppenz, M. Moehrle, F. Merget, S. Skacel, J. Witzens, S. Randel, W. Freude, and C. Koos, "Hybrid multi-chip assembly of optical communication engines by in situ 3D nano-lithography," Light Sci Appl **9**, 71 (2020). DOI: 10.1038/s41377-020-0272-5